J Sol-Gel Sci Technol (2015) 76:90–97
DOI 10.1007/s10971-015-3755-8

ORIGINAL PAPER

Controlling micro- and nanostructure and activity of the $NaAlO_2$ biodiesel transesterification catalyst by its dissolution in a mesoporous γ-Al_2O_3-matrix

Alexander V. Agafonov[1,4] · Inna A. Yamanovskaya[1] · Vladimir K. Ivanov[2,4] · Gulaim A. Seisenbaeva[3] · Vadim G. Kessler[3]

Received: 11 January 2015 / Accepted: 21 May 2015 / Published online: 29 May 2015

Abstract Mesoporous alumina and alumina–sodium aluminate composites were obtained by sol–gel method using polyethyleneimine as template. New approach for the regulation of the micro- and nanostructure of the composites as catalytic materials was proposed, exploiting inorganic seeds for the control of morphology for the produced nanostructures. Composition and temperature window for preventing the leaching of sodium aluminate in the course of reaction and thus drastically improving the catalytic activity has been identified. Structure and phase composition of the thus obtained catalytic materials were characterized using X-ray diffraction, N_2 adsorption/desorption, FTIR spectra, scanning electron microscopy, and thermal analysis. New type of catalyst has shown high efficiency in the vegetable oil transesterification process under mild conditions opening prospects for small-scale production of reasonably good-quality biodiesel fuel.

Graphical Abstract Dissolving sodium aluminate in the alumina matrix at proper compositions and under controlled temperatures permits to drastically decrease the leaching of aluminate and maintain its high catalytic activity in transesterification of vegetable oils with methanol.

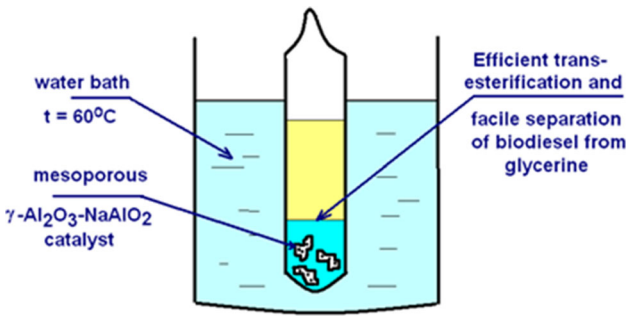

Keywords Sol–gel alumina · Template synthesis · Mesoporous matrix · Seeded crystallization · Transesterification catalyst · Biodiesel

Electronic supplementary material The online version of this article (doi:10.1007/s10971-015-3755-8) contains supplementary material, which is available to authorized users.

✉ Vadim G. Kessler
vadim.kessler@slu.se

Alexander V. Agafonov
ava@isc-ras.ru

Vladimir K. Ivanov
van@igic.ras.ru

Gulaim A. Seisenbaeva
gulaim.seisenbaeva@slu.se

1 Institute of Solution Chemistry, Russian Academy of Sciences, ul. Akademischeskaya 1, Ivanovo 153045, Russia

2 Kurnakov Institute of Inorganic and General Chemistry, Russian Academy of Sciences, Leninsky pr. 31, Moscow 117907, Russia

3 Department of Chemistry and Biotechnology, BioCenter, Swedish University of Agricultural Sciences, Box 7015, 75007 Uppsala, Sweden

4 National Research Tomsk State University, 634050 Tomsk, Russian Federation

1 Introduction

Biodiesel has recently attracted much attention as less polluting fuel obtained from renewable resources [1]. The major challenge in its broad-scale application is cost-efficient production of the fuel with sufficient quality. General approach to biodiesel is catalytic alkylation of vegetable

oils. Catalysts used in the transesterification of triglycerides are alkali, acid, enzyme or heterogeneous catalysts, among which alkali catalysts such as sodium hydroxide, sodium methoxide, potassium hydroxide, and potassium methoxide are considered more efficient [2]. In particular, the production of biodiesel from soybean oil by transesterification was carried out over sodium aluminate as heterogeneous catalyst [3]. Solid base showed high catalytic activity for methylation with methanol as reagent reaching a 93.9 % yield. As shown in [3], the aluminate has significant solubility in methanol, resulting in formation of soaps. Calcination of the aluminate decreases its solubility. However, with the increase in calcination temperatures, the basicity, solubility, and catalytic activity were also decreased. It has to be noted that solubility of sodium aluminate may also significantly increase when considerable water content is present in the methanol or in oil.

It is plausible to suppose that using a highly porous substrate, such as mesoporous matrix, for deposition of the sodium aluminate catalyst; it should be possible to maintain its high activity even when its solubility is decreased by calcination.

Mesoporous materials as a class of nanostructured materials are very perspective as catalysts and catalyst supports in heterogeneous catalysis. Mesoporous catalysts have large active surface area, good mechanical hardness, and very good hydrodynamic parameters for the contact with liquid phase [4–9]. Commonly mesoporous catalysts based on silica and even metal oxides are formed exploiting self-assembly of large organic surfactant or block copolymer molecules [4–9]. For metal oxide-based mesoporous solids an alternative to this approach are provided by self-assembly mechanisms guiding the aggregation of the primary oxometallate particles, MTSALs [10, 11]. An example of this type of approach has been described for the synthesis of γ-Al_2O_3 with the help of sodium salicylate as the source of small ligands for charging the surface of the primary particles [12].

The γ-Al_2O_3 is well known as a catalytically active material and catalyst support. Its catalytic activity is provided by the presence of Lewis and Brønsted acid and base centers [13–16]. Prospects of the future γ-Al_2O_3 applications are associated with its use as a biodiesel catalyst. A large number of catalytic systems for biodiesel production based on γ-Al_2O_3 have been studied, e.g., alkaline earth metal oxides/Al_2O_3, Li–CaO/Al_2O_3, La_2O_3/ZnO/Al_2O_3, La_2O_3/Al_2O_3, γ-Al_2O_3/ZrO_2, KI/Al_2O_3, NaOH/Al_2O_3, KF/Al_2O_3, etc. [3, 17–21] However, mesoporous structures based on the γ-Al_2O_3–$NaAlO_2$ system have to the best of our knowledge not been reported yet.

In our recent study [22], we showed possibility to obtain the wormlike mesoporous structure of γ-Al_2O_3 and of γ-Al_2O_3–CuO with high surface area and pore diameter of 8–12 nm, using polyethyleneimine (PEI) as template. PEI is a branched-chain water-soluble polymer which is widely used as pore-forming agent in the membrane fabrication [23]. This water-soluble polymer is defined as a pore-forming agent. The PEI has been applied as complexing template [22], which formed complexes with copper ions. It was thus possible to create high concentrations of copper ions in the mesopores of γ-Al_2O_3. Sol–gel process in that case was carried in acidic medium [22]. The structure of the PEI-copper complexes was proved to be linear. The difficulty and challenge in producing mesoporous γ-Al_2O_3–$NaAlO_2$ catalyst using the PEI template is that PEI in alkaline medium has the form of a coil.

The purpose of this work has been to develop a new approach to the synthesis of mesoporous γ-Al_2O_3–$NaAlO_2$ catalyst structures using combination of template and seed methods in sol–gel synthesis and finding the composition and temperature window for improvement of their activity through prevention of sodium leaching.

2 Experimental

All reagents, except water, were purchased from Sigma-Aldrich and used as received.

The boehmite sol was prepared by Yoldas method [24, 25] through peptization of aluminum hydroxide precipitate with nitric acid, as described in [26]. Stable boehmite sols were produced by mixing 16 g of aluminum iso-propoxide $Al(OC_3H_7)_3$ with 100 ml of deionized water, followed by peptization of the resultant white precipitate with 2 ml of concentrated nitric acid at 80 °C under vigorous stirring for 2 h (solution 1). The template solution was prepared by dissolving 4 g of the branched PEI, average $M_w \sim 25{,}000$ in 10 ml deionized water with stirring for 30 min at 40 °C (solution 2). Subsequently, the solution 1 was mixed at 80 °C with solution 2 under vigorous stirring and a yellowish gel was formed (solution 3). At the next step, $NaAlO_2$ was added at 80 °C to the solution (3) in 5, 10, 20, 40, 60, and 80 % fraction of the total catalyst weight (solution 4). Solution 4 was sonicated in an ultrasonic bath and evaporated in an air thermostat at 70 °C providing a dry solid. The mesoporous product has been obtained by calcination of the organic-containing samples at 600 °C for 3 h in air.

The dried and sintered samples were characterized by XPD using Bruker D8 Advance X-ray powder diffractometer with CuK_α radiation (15,478 Å), thermally with the NETZSH STA 409PC thermal analyzer, and by FTIR spectroscopy with Avatar 360 FTIR ESP instrument using KBr tablets, and by scanning electron microscopy with Hitachi TM-1000-μ-DeX instrument, and for high-resolution images, with Zeiss NVision 40 instrument. The specific surface area and pore size distribution of the catalyst samples were determined by multi-point BET and

BJH methods, using N_2 gas adsorption–desorption techniques (Quantachrome Nova 1200). The yield of esterification reaction was determined from quantitative ^{1}H NMR measurements using Bruker Avance 500 MHz instrument.

3 Results and discussion

The insight into the crystal structure of the produced catalysts was provided by the XRD studies. Figure 1a shows the XRD patterns of dry composite samples, with diffraction maximums of pseudo-boehmite (AlOOH) at $2\theta = 14°$; 28°; 38.5°; 49°. The increase in concentration of sodium aluminate leads to more distinct reflections of this latter phase with diffraction maxima at $2\theta = 18°$; 21°; 29°; 32°; 36°; 39°; 40° for the as-prepared sample [27].

Calcination at 600 °C leads to high extent of amorphization—only one broad peak of boehmite is visible at $2\theta = 47°$ (Fig. 1b). It is important to notice that the structure remains essentially amorphous independent of the calcinations time. Calcination at higher temperatures (the data for 950 °C is shown in 1d for the composite with 40 % of $NaAlO_2$) leads to re-appearance of clearly defined crystalline phases of both boehmite and sodium aluminate. The disappearance of the separate $NaAlO_2$ phase at intermediate temperature is most probably due to its intermediate dissolution (melting in) into the alumina phase. The morphology and porosity of the material remain unchanged at this intermediate temperature, but the leaching of $NaAlO_2$ is drastically decreased (for details see below) which gives rise to increased and stabilized catalytic activity.

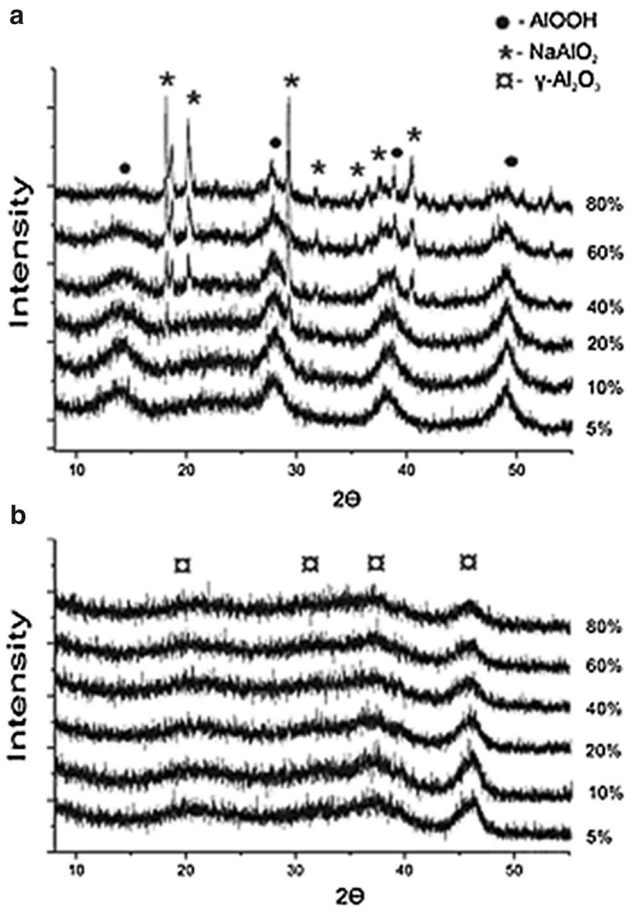

Fig. 1 XRD for samples in the γ-Al_2O_3–$NaAlO_2$ system with different content of $NaAlO_2$ **a** not calcined samples, **b** samples calcined at 600 °C

The morphological and chemical characteristics of the samples are compared in Fig. 2. General appearance of both the pure boehmite (Fig. 2a) and the composites with $NaAlO_2$ is gel-like, while the pure $NaAlO_2$ displays microcrystalline powder morphology (Fig. 2f). The most interesting feature of the produced gels is their different surface compositions for samples with different sodium aluminate content: both the samples with low and with high $NaAlO_2$ content do reveal sodium in the surface, while the intermediate content samples (40–60 % $NaAlO_2$) contain only aluminum in the surface layer.

This can be explained through different chemical behavior of sodium aluminate seed material dependent on its content. At low content (up to 20 %), the medium is predominantly acidic and the nucleation of the γ-Al_2O_3 occurs independently of the seeds, making the sodium content measurable. At the intermediate fraction (40–60 %), the medium becomes basic through leaching from the aluminate phase and the boehmite nanoparticles from the sol precipitate predominantly on the grains of $NaAlO_2$. At even higher content of the aluminate, the leaching is strong and can supposedly result in re-precipitation of $NaAlO_2$, resulting in growth of its grains together with boehmite and again in measurable concentration of sodium on the surface.

More detailed information about the micro- and nanostructure of the samples was provided by high-resolution SEM (see Fig. 3). It is clearly visible that the material in case of the catalytically most active samples with 60–80 % content of $NaAlO_2$ is a nanocomposite built up of larger microcrystals of γ-Al_2O_3 shaped as hexagonal rods and containing relatively much less sodium (below 1 wt%) together with a much more Na-rich nano powder (with single particles about 10 nm in size, forming wormhole mesoporosity via aggregation), where the phase of sodium aluminate, $NaAlO_2$, apparently is dominating. It can be hypothesized that the improved stability of the catalysts with intermediate sodium aluminate content is due to the dissolution of $NaAlO_2$ in mesoporous γ-Al_2O_3 crystals (as indicated by EDS). The basic centers are supposedly located in the pores within the alumina matrix and are rendered stable to leaching.

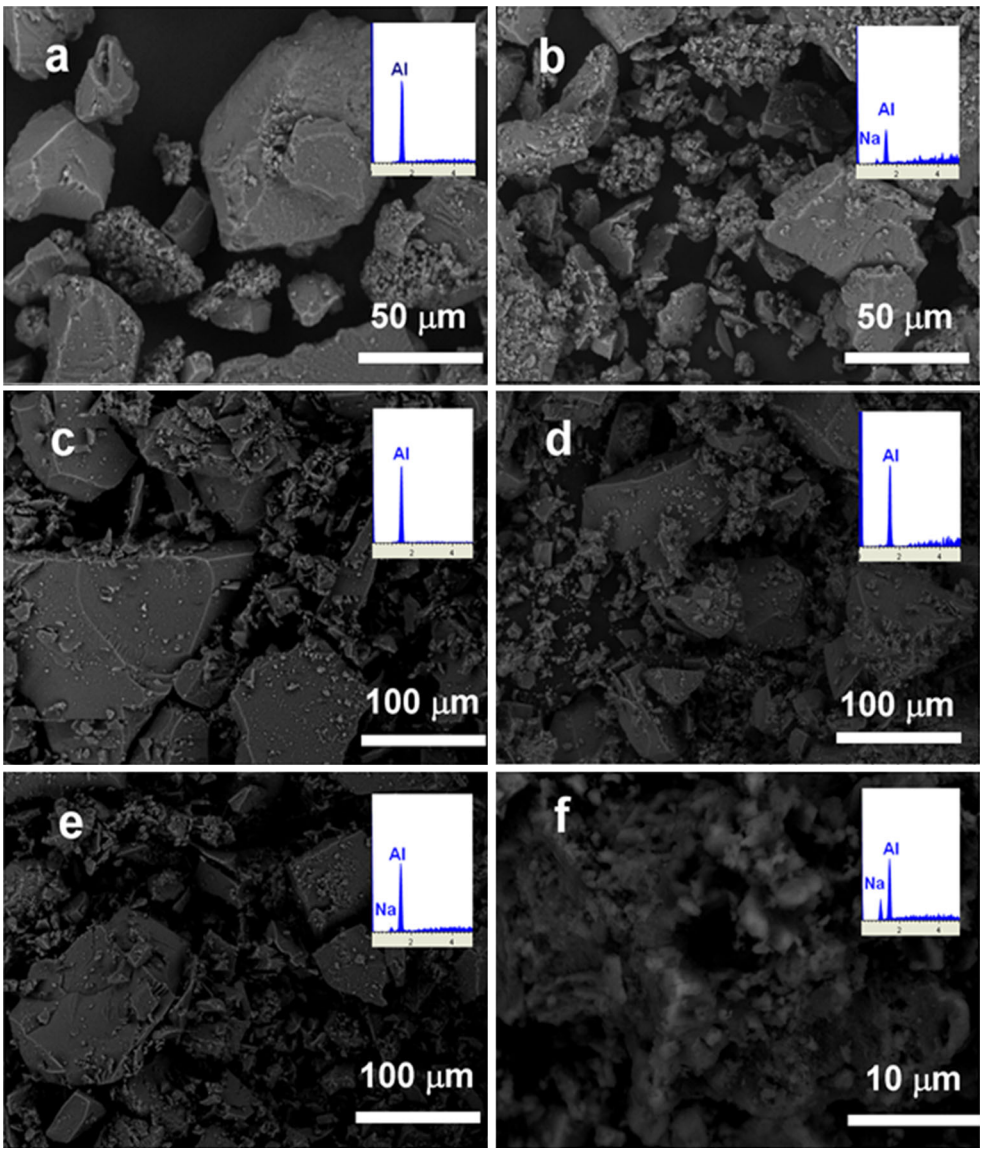

Fig. 2 SEM–EDS of the samples pure γ-Al_2O_3 (**a**); γ-Al_2O_3–$NaAlO_2$ with 20 % $NaAlO_2$ (**b**); 40 % $NaAlO_2$ (**c**); 60 % $NaAlO_2$ (**d**); 80 % $NaAlO_2$ (**e**); and pure $NaAlO_2$ (**f**)

The information about bonding in the as-prepared and calcined γ-Al_2O_3–$NaAlO_2$ samples can be obtained also from the FTIR spectra (see Fig. 4).

The spectra display peaks corresponding to stretching of the Al-O (peaks of 590 and 630 cm^{-1}) and Al–O–Al (750 and 800 cm^{-1}) bonds, bending vibrations of H_2O molecules (1620, 1630 cm^{-1}) and of hydroxyl—OH groups (1550 cm^{-1}). The broad band in the area 2850–3490 cm^{-1} reveals existence of nonequivalent molecules of water, –OH groups, and hydrogen bonds. Peaks at 1350 and 1370 cm^{-1} correspond to stretching of the C–H fragments. Bands at 2900 and 2910 cm^{-1} reveal existence of CH_2-groups which partially remain even after calcination.

The provided absorption bands can be observed in the spectra of both calcined and not calcined samples, the difference been in appearance of the Al–O–Na (1015 cm^{-1}) bands, qualitatively proving existence of an active phase in not calcined samples.

The porosity and surface area in the heat-treated samples were investigated by nitrogen sorption experiments (see Fig. 5). In all cases, it is apparent that the powders exhibit classical type-IV isotherm curves with a hysteresis loop, according to the IUPAC classification [28]. The active surface area and porosity of the pure γ-Al_2O_3 samples was quite resemblant of the values reported in [12] for self-assembled mesoporous alumina.

As it can be seen in Fig. 5, the content of $NaAlO_2$ in composites affects significantly the structure of resulting materials. With increasing $NaAlO_2$ concentration up to 40 %, a displacement of the start of the hysteresis loops

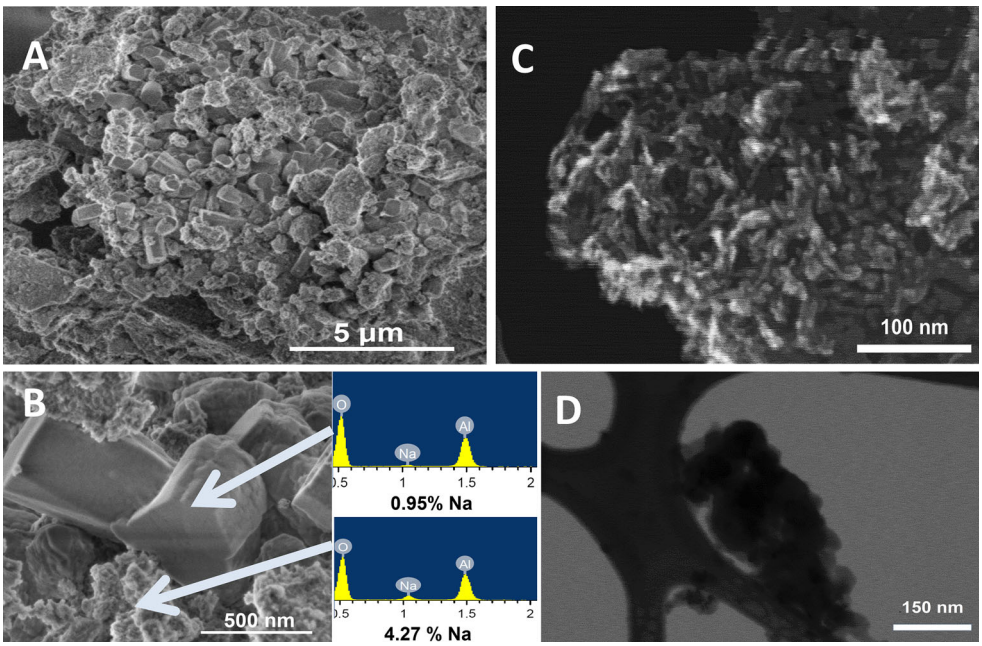

Fig. 3 High-resolution SEM (**a, b**) together with EDS (*inset*), high-resolution STEM (**c**), and TEM (**d**) of the 60 % $NaAlO_2$—γ-Al_2O_3 sample calcined at 600 °C

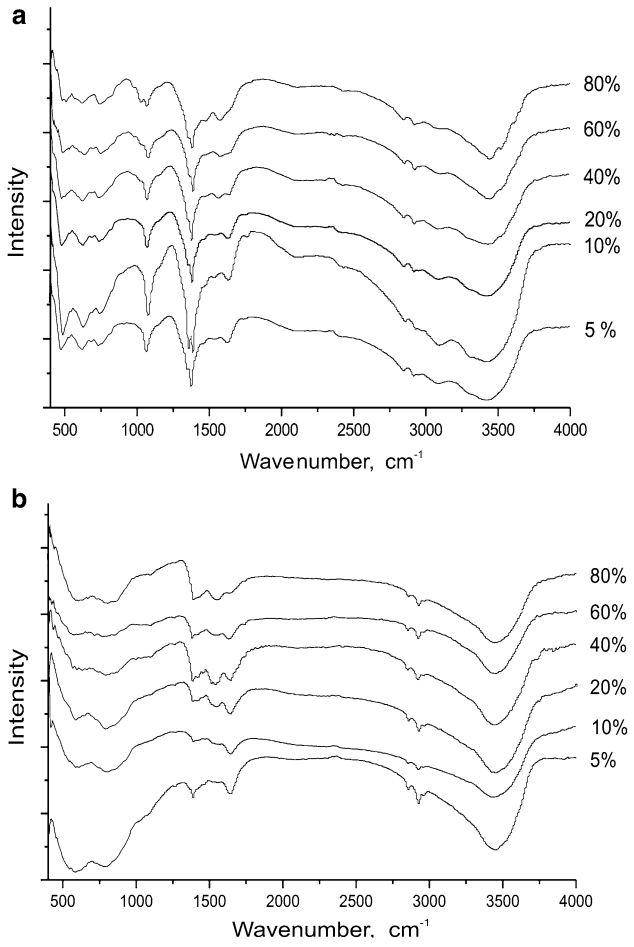

Fig. 4 FTIR spectra for samples in the γ-Al_2O_3–$NaAlO_2$ system with various contents of $NaAlO_2$ **a** not calcined samples, **b** calcined at 600 °C

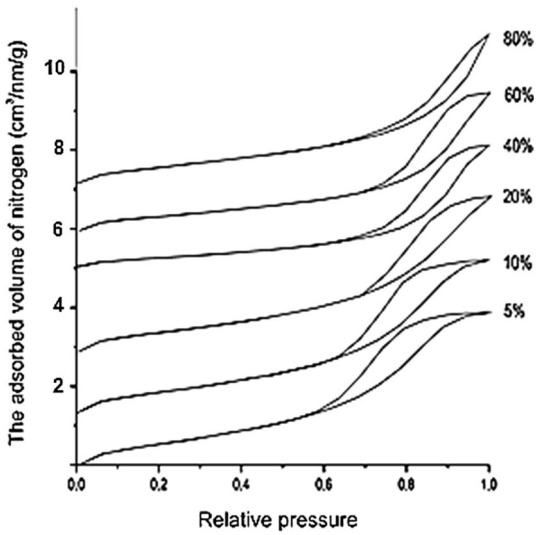

Fig. 5 Nitrogen adsorption–desorption isotherms for samples of the γ-Al_2O_3–$NaAlO_2$ system with different contents of $NaAlO_2$, calcined at 600 °C

along the P/P_0 axis from 0.57 to 0.7 is observed. Further increase in the content of $NaAlO_2$ leads to reverse in the displacement of hysteresis loops that also change form. The pores of slits type presumably have been formed instead of wormlike cylindrical pores in the materials (for BET and BJH pore size distribution, please, see Table 1; Fig. 6).

When the dry samples with 5 % $NaAlO_2$ were calcined at 600 °C for 2 h, the highest specific surface area, 262 m^2/g, was obtained with the corresponding pore volume of 0.48 cm^3/g and average pore size of 7.4 nm.

The increase in the $NaAlO_2$ content from 5 to 80 % is associated with decrease in the specific surface area from 262 m^2/g to 91 m^2/g, and the pore volume decrease from 0.48 to 0.19 cm^3/g, but the pore diameter increases at the same time from 7.4 to 20 nm. This effect can be ascribed to the state of the polyethyleneimine in the composites with different contents of $NaAlO_2$ and to the structural changes on the polyethyleneimine removal.

Thermogravimetric and differential thermal analyses of as-sintered dry Al_2O_3–$NaAlO_2$ samples containing 40, 60, and 80 wt% $NaAlO_2$ were performed at the heating rate of 5 °C/min (see Fig. 7). The thermal transition of boehmite to γ-Al_2O_3 [29] has been associated with the following effects in the DTA curve: (1) loss of physically bound water—a peak near 90 °C; (2) loss of chemically bound water—a peak near 200 °C; (3) transformation of boehmite into γ-Al_2O_3 (or transitional form)—the peak near 380 °C; and (4) dehydration of the residual hydroxide groups finishing with crystallization of the alpha alumina. The last step gives no thermal event, but appears as a continuous mass loss and seems to stop at about 900 °C.

In the Fig. 7, the first endothermic peak in the DSC curve is associated with the loss of physically bound water. For the $NaAlO_2$ concentration of 40, 60, and 80 %, the DSC curves display double peaks with maxima at 200 and 300 °C. The first peak can be associated with the loss of chemically bound water. The second peak is corresponding to the thermal degradation of the PEI molecules adsorbed on the outer surface of the inorganic particles. Small exothermic peak with a maximum near 400 °C may be associated with the transition of boehmite into the γ-Al_2O_3. Exothermic peak at 500 °C can be attributed to the combustion of polyethyleneimine, entrapped in the matrix of aluminum oxide. This peak is revealed only for the compositions that contain 40 and 60 % of $NaAlO_2$. This may indicate different mechanisms of action of template in these systems. At the $NaAlO_2$ content of 40 and 60 %, large portions of PEI were included in the inorganic matrix. With 80 % content of $NaAlO_2$, all PEI molecules are on the surface of the inorganic particles and are not involved in the formation of mesophases.

Commercial edible-grade canola oil as the source for catalytic tests in biodiesel production was obtained from

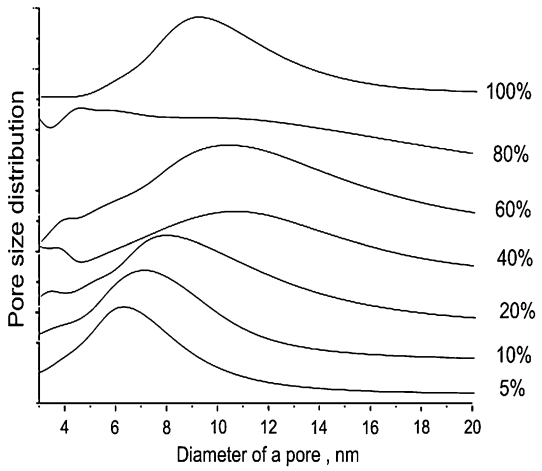

Fig. 6 Pore size distribution in the γ-Al_2O_3–$NaAlO_2$ sample calcined at 600 °C depending on the concentration of $NaAlO_2$

the market. The transesterification process has been performed in a 10 cm^3 sealed glass bottle with the oil/methanol = 1:5 molar ratio, and 0.2 g of catalyst at 60 °C. The water content in methanol was 1 %. The mixture was kept under stirring for 0.5, 2, 4, and 6 h. After the reaction, the solid catalyst was separated by filtration. The liquid was put into a graded glass tube and was kept at ambient temperature for 24 h, which resulted in two liquid phases. The upper layer was biodiesel, and the lower layer was glycerin. The transesterification products were analyzed according to [30–33]. The biodiesel was characterized by ^1H NMR spectroscopy, and its spectrum in $CDCl_3$ is shown in Figure FS 1. The characteristic peak of methoxy protons was observed at 3.64 ppm and of the α-CH_2 protons at 2.288 ppm. ^1H NMR has been used to quantify the conversion of vegetable oil to methyl esters by transesterification reaction. The equation used to quantify the yield of transesterification was according to [32, 33]:

$$C = 100 \times 2AMe/3ACH_2$$

where C is percentage conversion of triglycerides to corresponding methyl esters; AMe is peak area for the methoxy protons of the methyl esters, and ACH_2 is the peak area for carbonyl methylene protons (see Fig. FS1).

The best catalytic activities were displayed by the catalysts with 40 and 60 % of $NaAlO_2$. In the oil–methanol

Table 1 Textural characteristics of samples in the Al_2O_3–$NaAlO_2$ system heat-treated at 600 °C

$NaAlO_2$ content (%)	S_{BET} (m^2/g)	$S_{BJH\ meso}$ (m^2/g)	V_{pore} (cm^3/g)	D_{pore} (nm)
5	262	299	0.48	7.4
10	240	274	0.46	7.7
20	207	207	0.43	8.3
40	144	161	0.42	11.0
60	119	144	0.33	11.6
80	91	62	0.19	20

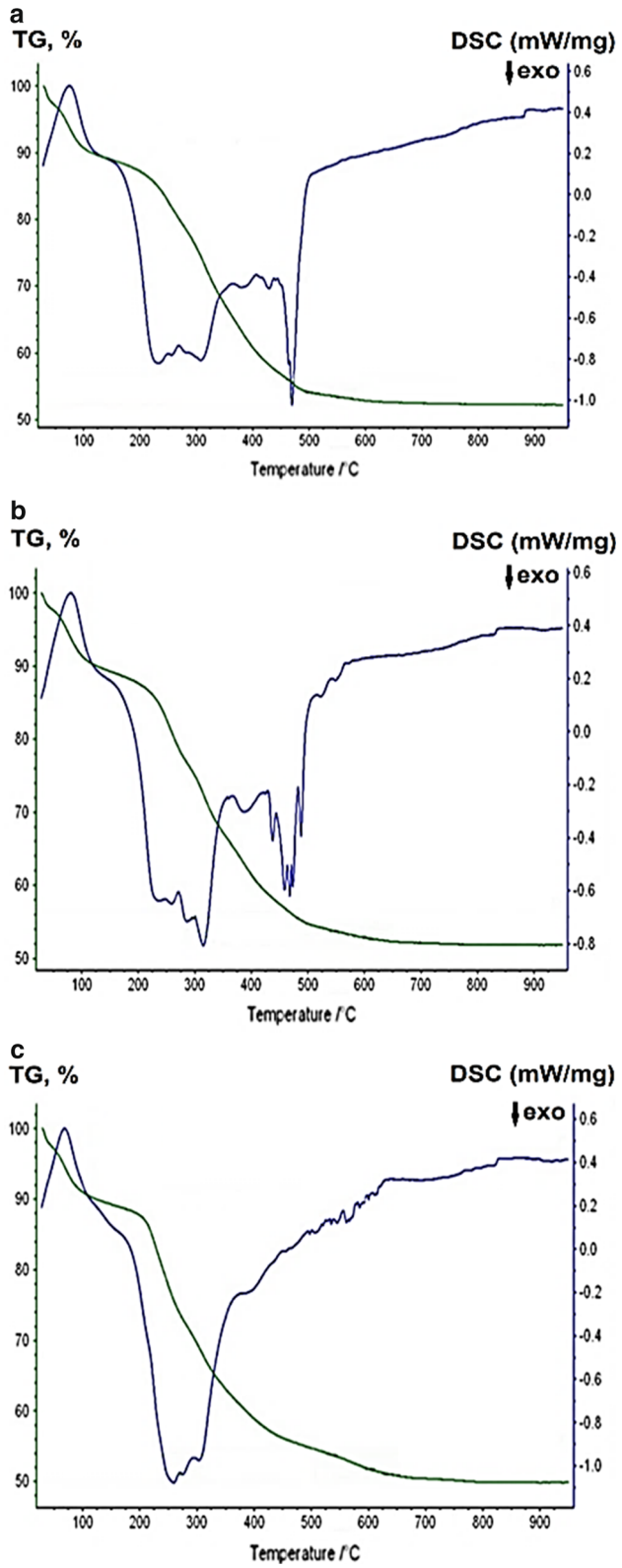

Fig. 7 TG and DSC of the γ-Al_2O_3–$NaAlO_2$ sample with 40 % $NaAlO_2$ content (**a**); with 60 % $NaAlO_2$ (**b**); with 80 % $NaAlO_2$ (**c**)

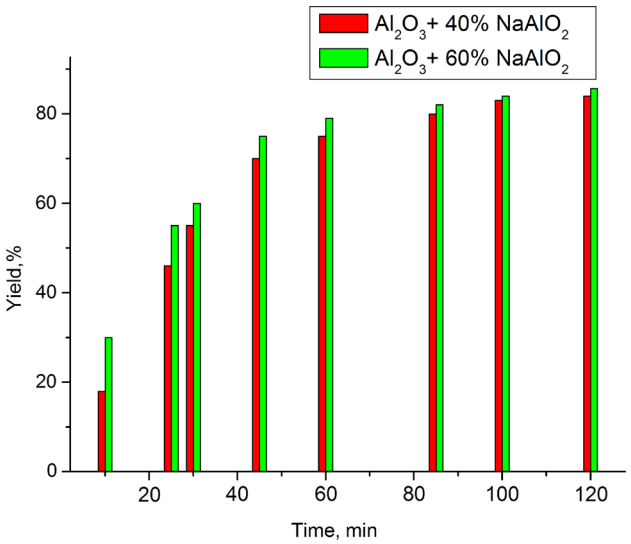

Fig. 8 Conversion of the sum of triglycerides in time for the processes over catalysts with 40 and 60 % of $NaAlO_2$ at 60 °C

system using the catalyst with 80 % $NaAlO_2$, the soap formed as major product of the reaction. Oil–biodiesel conversion using a catalyst containing 60 % of the $NaAlO_2$ reached 60 % in 30 min and increased to about 85.7 % within 2 h (see Fig. 8).

The FTIR spectra can be used to estimate the quality of the biodiesel from transesterification of canola oil (Fig. FS2). The strong ester peaks at 1750 cm^{-1} (C=O ester) and at 1170–1200 cm^{-1} (C–O ester) are clearly present in the spectra together with the characteristic peak of the CH_3-group in the methyl ester at 1445 cm^{-1}. FTIR spectra of pure glycerin from Sigma-Aldrich and glycerin as produced in the transesterification process correlate well with each other. The selectivity of transformation into methyl esters is at 60 °C about 64 % and increases rapidly with the increase in temperature making the process attractive for the small-scale production of biodiesel.

4 Conclusions

Mesoporous alumina–sodium aluminate composite materials have been successfully produced by templating-and-seeding sol–gel method. The sodium aluminate micro powder was introduced directly into the sol of aluminum oxide and acted as seeding material. Depending on the synthesis conditions and the content of sodium aluminate, the materials with different active surface area (from 91 to 262 m^2/g), pore size (from 7 to 20 nm), and pore volume (from 0.19 to 0.48 cm^3/g) were produced. The freshly

prepared material has according to X-ray diffraction predominantly the pseudo-boehmite structure that transforms into γ-Al_2O_3 on the heat treatment required for the template removal. The thermal window for dissolution of sodium aluminate in the alumina matrix permitting to drastically decrease the leaching of aluminate and maintain its high catalytic activity has been identified. The resulting material revealed high catalytic activity in transesterification of vegetable oils with methanol. The conversion of oil into methyl esters of fatty acids reached 85.7 % after 2 h at 60 °C. This simple approach opens prospects for small-scale production of reasonably good-quality biodiesel fuel.

Acknowledgments The authors express their gratitude to the Russian Ministry of Higher Education and Science for the visiting scientist at ISC RAS grant to Vadim Kessler.

References

1. Balat M, Balat H (2008) Energy Convers Manag 49:2727–2741
2. Meher LC, Sagar DV, Naik SN (2006) Renew Sustain Energy Rev 10:248–268
3. Wan T, Yu P, Wang S, Luo Y (2009) Energy Fuels 23:1089–1092
4. Frost R, Zhu HY, Wu P, Bostrom T (2005) Mater Lett 59:2238–2241
5. Kresge CT, Leonowicz ME, Roth WJ, Vartuli JC, Beck JS (1992) Nature 359:710–712
6. Bagshaw SA, Prouzet E, Pinnavaia TJ (1995) Science 269:1242–1244
7. Corma A (1997) Chem Rev 97:2373–2419
8. Taguchi A, Schuth F (2005) Micropor Mesopor Mater 77:1–45
9. Cejka J (2003) Appl Catal A Gen 254:327–338
10. Kessler VG, Spijksma GI, Seisenbaeva GA, Håkansson S, Blank DHA, Bouwmeester HJM (2006) J Sol Gel Sci Technol 40:163–179
11. Seisenbaeva GA, Kessler VG (2014) Nanoscale 6:6229–6244
12. Patra AK, Dutta A, Bhaumik A (2012) J Hazard Mater 201–202:170–177
13. Trimm DL, Stanislaus A (1986) Appl Catal 21:215–238
14. Yada M, Machida M, Kijima T (1996) Chem Comm 769–770
15. Yada M, Kitamura H, Machida M, Kijima T (1997) Langmuir 13:5252–5257
16. Yada M, Hiyoshi H, Ohe K, Machida M, Kijima T (1997) Inorg Chem 36:5565–5569
17. Peng-Lim B, Gaanty PM, Shafida AH (2011) Chem Eng J 168:15–22
18. Watkins RS, Adam FL, Wilson K (2004) Green Chem 6:335–341
19. Chai F, Cao F, Zhai F, Chen Y, Wang X, Su Z (2007) Adv Synth Catal 349:1057–1065
20. Boz N, Kara M (2008) Chem Eng Comm 196:80–92
21. Refaat AA (2011) Int J Environ Sci Tech 8:203–221
22. Vinogradov VV, Agafonov AV, Vinogradov AV, Guliaeva TI, Drozdov VA, Licholobov VA (2010) J Sol Gel Sci Technol 56:333–339
23. Xiang T, Zhao L, Li Y, Lei Z, Jin S, Li S, Li Y, Liang Y (2008) Mater Lett 62:1627–1629
24. Yoldas BE (1975) Am Ceram Soc Bull 54:286–288
25. Yoldas BE (1973) J Appl Chem Biotechnol 23:803–809
26. Pai RV, Pillai KT, Pathak S, Mukerjee SK, Vinogradov VV, Agafonov AV, Vinogradov AV, Aggarwal SK (2012) J Sol Gel Sci Tech 61:192–196
27. Rodgers KA, Gregory MR, Barton R (1991) Clays Clay Miner 39:103–107
28. Kaneko K (1994) J Membr Sci 96:59–89
29. Alphonse P, Courty M (2005) Thermochim Acta 425:75–89
30. Mahamuni NN, Adewuyi Y (2009) Energy Fuels 23:3773–3782
31. Tariq M, Ali S, Ahmad F, Ahmad M, Zafar M, Khalid N, Ajab Khan M (2011) Fuel Proc Tech 92:336–341
32. Gelbard G, Bres O, Vargas RM, Vielfaure F, Schuchardt UF (1995) J Am Oil Chem Soc 72:1239–1241
33. Knothe G (2000) J Am Oil Chem Soc 77:489–493